THEORETICAL INVESTIGATION OF POLAR ZINC OXIDE SURFACE MODIFICATION VIA PHOSPHONIC ACID SELF-ASSEMBLED MONOLAYERS

A Dissertation
Presented to
The Academic Faculty

By

Christopher Alan Wood

In Partial Fulfillment
Of the Requirements for the Degree of
Master of Science in Chemistry

Georgia Institute of Technology

May 2012

THEORETICAL INVESTIGATION OF POLAR ZINC OXIDE SURFACE MODIFICATION VIA PHOSPHONIC ACID SELF-ASSEMBLED MONOLAYERS

Approval:

Dr. Jean-Luc Brédas, Advisor
School of Chemistry & Biochemistry
Georgia Institute of Technology

Dr. David Sherrill
School of Chemistry & Biochemistry
Georgia Institute of Technology

Dr. Angelo Bongiorno
School of Chemistry & Biochemistry
Georgia Institute of Technology

Date Approved: January 10th, 2012

ACKNOWLEDGEMENTS

I would like to first and foremost thank my thesis advisor, Dr. Jean-Luc Brédas, for his insight and guidance through my years here at Georgia Tech. I would also like to thank Dr. Hong Li and Dr. Paul Winget for the significant support they each provided for my work. I would like to thank Dr. David Sherrill and Dr. Angelo Bongiorno for their approval of my thesis and for the conversations we had following my oral examinations. Recognition also goes to Solvay for providing the initial financial support and the American Recovery and Reinvestment Act (Department of Energy, Energy Frontier Research Center) for funding the final segment of my research. My time at Georgia Tech has been the most intellectually-rewarding period of my life, and part of me is sad to see it come to an end. However, as I gaze towards the future, I know that the skills and knowledge I have gained will serve me well in whatever career path I choose to follow.

TABLE OF CONTENTS

LIST OF TABLES

LIST OF FIGURES

LIST OF ABBREVIATIONS

BD	Bond Dipole
BPA	Benzylphosphonic Acid
CB_{min}	Conduction Band Minimum
DFT	Density Functional Theory
ET	Electron Transfer
GGA	Generalized-Gradient Approximation
ITO	Indium Tin Oxide
IZO	Indium Zinc Oxide
OLED	Organic Light-Emitting Diode
OPV	Organic Photovoltaic
PA	Phosphonic Acid
PAW	Projector-Augmented Wave
PBE	Perdew-Burke-Ernzerhof
PDOS	Partial Density of States
PPA	Phenylphosphonic Acid
SAM	Self-Assembled Monolayer
TFT	Thin Film Transistor
VASP	Vienna Ab Initio Simulation Package
VB_{max}	Valence Band Maximum
XPS	X-ray Photoelectron Spectroscopy

SUMMARY

The interface of a zinc-terminated polar zinc oxide surface (0002) with a series of chemisorbed fluorinated benzylphosphonic acids has been studied using density functional theory. The calculations indicate that there is a substantial change in the binding energies and modification of the work function depending on the binding motif. The results also indicate that there is a pronounced difference in the magnitude and trends of the factors determining the total change in work function with respect to the unmodified surface. Binding energies were calculated for two thermodynamically-favored binding modes and compared to experimental data. The 1s core-level binding shifts for the oxygen atoms in the PO_3 moiety with respect to the oxygen in the bulk zinc oxide were calculated; these relative shifts were compared to experimental XPS data as a method to identify the presence of the two binding modes modeled.

In the following chapter, a series of *para*-substituted benzyl- and phenyl- phosphonic acid self-assembled monolayers (SAMs) chemisorbed to an identical zinc-terminated ZnO surface have been modeled in the thermodynamically-favored tridentate binding mode established in the prior chapter. The change in surface work function upon deposition of the SAMs has been determined, with each of its contributing terms calculated independently. In addition, the relationship between the modeled gas-phase molecular dipole and the molecular dipole normal to the surface for each SAM was established; as a primary contributor to the variance in the work function with respect to the choice of molecular SAM, a stronger understanding of this relationship and its

contributions to the observed surface work function will further aid in the design of phosphonic acid surface modifiers for future device applications.

CHAPTER 1-

INTRODUCTION

Advancements in organic electronic technologies have emerged from the research and development efforts in a wide variety of scientific disciplines including chemistry, physics, materials science and device engineering. Compared to typical silicon-based semiconductors, organic electronic materials possess a number of unique properties: firstly, they can be designed for physical flexibility through deposition onto flexible substrates.[1-3] In addition, the methods used to create the materials can be custom tailored or tuned, granting scientists and engineers the ability to design, via traditional synthetic chemistry techniques, organic molecular systems with varying semiconducting properties, solubility in different solvents, and the color of the light emitted or absorbed.[4,5]

For industrial applications, solution-processable organic semiconductors have the potential to lead to significant cost savings compared to traditional silicon-based devices. Organic semiconductors can be deposited from solution via more versatile and economic techniques, such as spin coating, drop casting, or inkjet printing.[6,7] These techniques are leading towards the low-cost mass production of new generations of thin-film electronic devices such as organic light-emitting diodes (OLEDs), photovoltaics (OPVs), and field-effect transistors (OFETs).[8,9] In addition, organic electronic materials could lead to devices with lower power consumption versus their inorganic counterparts, especially in the areas of displays and large-area lighting.[10] The combination of these attributes has

fueled research and development in organic electronics in laboratories across both academia and industry.

1.1 Organic Light-Emitting Diodes

The field of organic electronics can trace its origins to the 1977 discovery—by Alan J. Heeger, Alan G. MacDiarmid, and Hideki Shirakawa—of the conducting properties of doped polyacetylene.[11] In this work, they demonstrated that organic conjugated polymers can present metallic-like electrical conductivity upon chemical doping. These conducting polymers have unique characteristics, combining the electrical properties of metals with the mechanical properties of polymers. For this revolutionary discovery, the three were awarded the 2000 Nobel Prize in Chemistry.

The pursuit of organic electronic materials for OLEDs began in 1963 when Pope and co-workers[12] discovered electroluminescence in organic crystals. However, due to the high voltage requirement, there was little interest in the field until 1987 when Tang and VanSlyke[13] at Kodak reported an efficient, low-voltage electroluminescent device based on a π-conjugated material, tris(8-hydroxy-quinoline) aluminum (Alq3). Shortly afterwards, Friend and co-workers[14] at the University of Cambridge constructed a similar device using a conjugated polymer, poly(para-phenylenevinylene) (PPV), as the organic emitter. Since that time, rapid developments in organic materials have led to new generations of thinner high-resolution displays for computers, televisions, and hand-held devices. Unlike traditional liquid-crystal displays (LCDs), OLEDs generate their own light and thus do not require backlighting for screen illumination, making these devices

lighter and thinner. Furthermore, OLEDs offer a host of other advantages over LCD technology, including lower power requirements, faster response times, wider viewing angles, and higher brightness and contrast ratios.

A typical OLED architecture (see Figure 1), consists of an anode, such as indium tin oxide (ITO), deposited onto a transparent substrate. The emissive organic layer is sandwiched between two conducting layers: a hole injection layer and an electron transport layer. At the top, there is a reflective metal cathode. When a bias is applied between the two electrodes, holes are injected from the anode and migrate through the hole injection layer, while electrons are injected from the cathode and move through the electron transport layer. When the holes and electrons meet at the interfacial region, they recombine to form a bound electron-hole pair: an exciton. Relaxation of the exciton to the ground state (the electron filling the hole) gives rise to light emission.

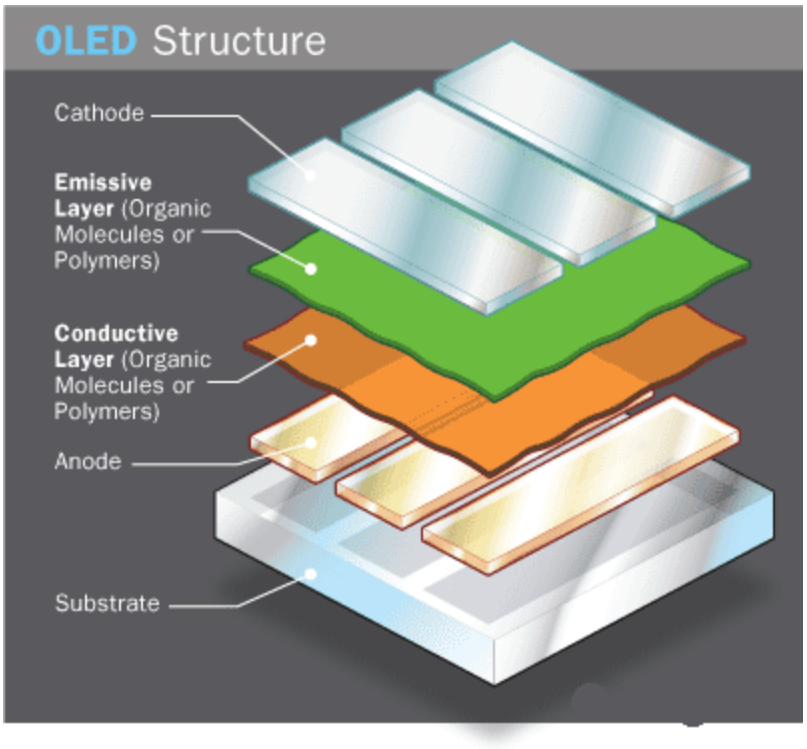

Figure 1. Depiction of the architecture of a traditional OLED device[15]

To summarize, as shown in the top portion of Figure 2, there are 5 main steps for light generation: (i) charge injection at the two electrodes; (ii) hole and electron transport through their respective organic layers; (iii) charge recombination (exciton formation) at the interfacial region; (iv) energy transfer; and (v) light emission. The organic emissive layer is made of a π-conjugated material that can be either a small molecule or a polymer, with the color of emitted light dependent on the composition of the organic material. A combination of red, green, and blue emissive materials can be used together to produce the full color spectrum.

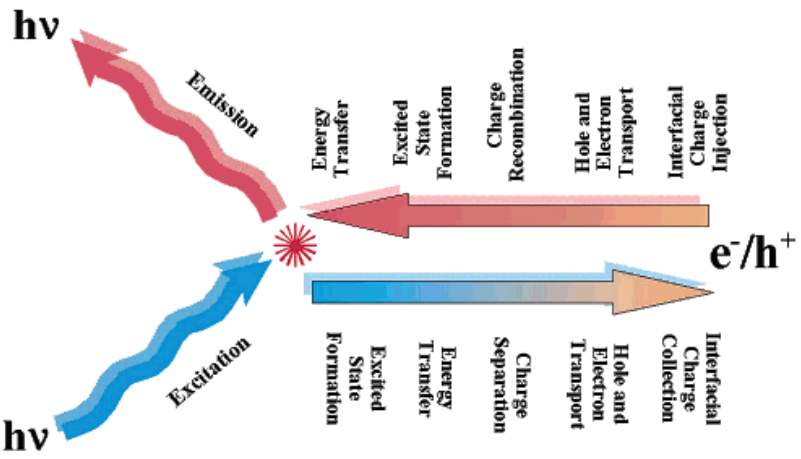

Figure 2. A basic overview of the fundamental processes that occur within a OLED (red line, above) and a OPV device (blue line, below)[16]

1.2 Organic Photovoltaics

Over the past decade, advances in solar power conversion efficiencies have opened new pathways to organic-based photovoltaics (OPVs) as a low-cost method for power generation;[17] harvesting energy from the sun using photovoltaic cells will be an essential component of future global energy production. The photovoltaic effect was discovered by 19-year old French physicist Alexandre-Edmond Becquerel in 1839, but commercialization did not start until 1954, when the first crystalline Si photovoltaic (PV) device was developed at Bell Laboratories.[18]

OPV devices have a similar architecture to that of OLEDs, although they perform the inverse process: the dissociation of a photoexcited state via charge separation instead of the creation of an excited state via charge recombination (as is the case for OLEDs). Consequently, as depicted in the bottom half of Figure 2, there are again five main steps that occur in PV devices:[19] first, light is absorbed within the organic layers, generating

exciton charge carriers. Second, these excitons migrate towards the interfacial region between the organic layers. The third step involves charge dissociation through photoinduced electron-transfer (ET),[20] with the exciton separating into its component electron and hole. The fourth step involves the now-separated charges each migrating towards their respective electrodes, accelerated by the electric field. In the fifth and final step, charge collection occurs at the electrodes, allowing the device to drive an external circuit.

1.3 Self-Assembled Monolayers

Organic molecules can readily form self-assembled monolayers (SAMs) on metals, metal oxides, and semiconductors, providing a simple, convenient, and versatile system for tuning the interfacial electronic properties of a wide range of surfaces. SAMs are promising components in high-performance, low cost, and flexible electronic devices, since the spontaneous process of self-assembled film formation has the advantages of substrate selectivity and the ability to readily form densely-packed monomolecular films over a large area. The nearly infinite structural variety of organic molecules available makes them an attractive option for modifying metal oxides due to the vast array of options it provides to chemists and material scientists. These devices have been of significant interest in the areas of sensing, [21,22] display technologies,[23-26] and other electronic applications; they offer inexpensive alternatives and possess their own sets of interesting bulk and surface properties.

The SAM-surface interfacial region is of particular importance in many electronic devices; for example, in organic thin film transistor (TFT) devices, ~95% of the charge transport in the semiconductor channel occurs within the first few layers of semiconductor molecules at the semiconductor/dielectric interface.[27] Robust, dense monolayers of aromatic silanes on SiO_2 have been used to develop such TFT devices.[28] Carboxylic and phosphonic acid SAMs have been used to form favorable functionalized surfaces on a variety of metal oxide nanocrystals and surfaces, including TiO_2,[29-32] Al_2O_3,[33] and ITO[34]. Triphenylamine-based carboxylic acids SAMs were modeled as an organic modifier for a TiO_2 electrode to develop a better chromophore for dye-based solar cells[35,36].

Phosphonic acids have proven to form stronger bonds than carboxylic acids on a wide range of these metal oxides, forming well-packed SAMs with excellent thermal stability. Phosphonic acid SAMs have been used to modify the work function of $BaTiO_3$ surfaces[37] and nanoparticles[38] for use in organic field-effect transistor devices. Microcontact printing techniques have been combined with wet chemical etching to use phosphonic acid SAMs to fabricate electronic structures on thin films of ITO and IZO.[39]

In the next chapter, the methodology used to model a series of phosphonic acid (PA) monolayers on the polar (0002) ZnO surface will be described, along with the calculations for the change in work function and the decomposition of its major contributing factors. In the following chapter, the binding energies and work functions are modeled for a series of fluorinated PA monolayers in two different binding geometries. In the final chapter, the work function contributions are computed for a

series of *para*-substituted phosphonic acid monolayers in the energetically-favored tridentate binding mode found in the prior chapter. The last section of this thesis contains a brief discussion on future directions for this work.

CHAPTER 2-

METHODOLOGY

2.1 Computational Method

The calculations were carried out at the DFT level using the Vienna Ab Initio Simulation Package (VASP).[40,41] As in previous work in our research group, we make use of the generalized-gradient approximation (GGA) exchange-correlation functional of Perdew, Burke, and Ernzerhof (PBE)[42,43] and the projector-augmented wave (PAW) method.[44] An energy cut-off of 400 eV is applied in all instances. The tetrahedral smearing with Blöchl corrections[44] with σ=0.1 eV was used for the Brillouin-zone integrations on a 2x2x1 k-point mesh. The total energy convergence for the self-consistent iterations is set at 10^{-6} eV and the maximal residual force on each atom in the course of geometry optimizations is 0.02 eV/Å. The GGA+U approximation[45] with an effective Hubbard U-parameter (U_{eff} = 8.5 eV)[46] is applied to describe the strongly localized zinc 3d-orbitals. This particular U-parameter was selected to match the energy levels of the calculated zinc 3d-orbitals to those found in experiment, preventing the mixing of those orbitals with the oxygen 2p-orbitals at the top of the valence band. Earlier work showed that this parameter resulted in a calculated band gap of 1.8 eV,[47] which is still much smaller than the experimental value of 3.3-3.4 eV.[48]

2.2 Core-Level Binding Energy Shifts

The O(1s) core-level binding energy shifts for the three PA oxygen atoms were calculated using the method developed by Köhler and Kresse.[49,50] The method, which

calculates the difference in energy required to remove a core electron from an atom, can be compared to the binding energy shift determined experimentally by X-ray photoelectron spectroscopy (XPS). For the purposes of this study, the shift in core-level binding energy between the PA oxygen atoms and the oxygen atoms in the bulk ZnO were determined using the following method:

$$E_{\mathrm{SCLS}} = [E_{\mathrm{surface}}(n_c - 1) - E_{\mathrm{surface}}(n_c)] - [E_{\mathrm{bulk}}(n_c - 1) - E_{\mathrm{bulk}}(n_c)] \quad (1)$$

Where $E_{surface}(n_c)$ is the total energy of the PA-ZnO system at the unexcited ground state, $E_{surface}(n_c\text{-}1)$ is the total energy of the system with a 1s core electron of the oxygen belonging to the PO_3 moiety removed and added to the conduction band; the two E_{bulk} terms represent the same values for the bulk-like ZnO, taken from an oxygen atom located in the third ZnO layer of the unmodified surface in the same unit cell.

2.3 Evaluating the Change in Work Function

The work function, Φ, can be defined as the energy required to move an electron from a surface into the vacuum above it, and can be represented as follows:

$$\Phi = V_{vac} - E_{\mathrm{F}} \quad (2)$$

Where V_{vac} is the plane-averaged electrostatic potential energy of an electron in the vacuum region above the surface, sufficiently far away to have reached an asymptotic value, and E_F is the Fermi energy of the system. Due to the naturally-occurring n-type semiconductor properties of ZnO,[51,52] the conduction band minimum was used as the effective Fermi level for calculating the work function. An example of this calculation is

depicted in Figure 3 for a benzyl-PA monolayer modeled on ZnO: the plane-averaged electrostatic potential normal to the surface is plotted through the system, and the difference between this value in the vacuum above the surface and the Fermi level (the calculated conduction band minimum), shown as a red line. The difference between these two values gives the work function, Φ. By comparing this value to the calculated work function for the unmodified surface, a change in work function ΔΦ can be evaluated and used for comparison between different molecular monolayers.

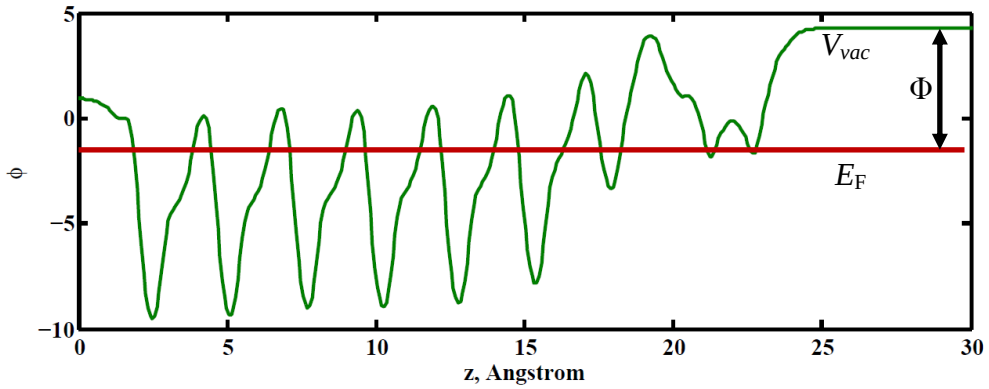

Figure 3. A depiction of the calculated work function for the tridentate-bound benzyl-PA on the polar (0002) ZnO surface, calculated as the difference between the electrostatic potential (green line) in the vacuum region above the system and the Fermi energy (red line).

2.4 Decomposition of the Work Function

The work function change was decomposed into its contributing components:

$$\Delta\Phi_{\text{calc}} \approx \Delta V_{vac} + \text{BD} + \Delta\Phi_{\text{geo}} = \Delta\Phi_{\text{tot}} \quad (3)$$

where ΔV_{vac} is the potential energy change of an electron crossing the isolated molecular SAM at the same geometry as adsorbed on the ZnO surface, BD (bond dipole) is the potential energy shift of an electron due to the charge redistribution occurring at the very interface of the PA-SAM and the ZnO slab, and $\Delta\Phi_{geo}$ is the change in the work function of bare ZnO surface due to geometry reorganization upon chemisorption of the SAM. The sum of these terms, $\Delta\Phi_{tot}$, can be compared to the calculated value $\Delta\Phi_{calc}$ to demonstrate the consistency and accuracy of this method.

The bond dipole was calculated by solving Poisson's equation, using the change in plane-averaged electron density normal to the surface $\Delta\rho(z)$:

$$\Delta\rho(z) = \rho_{\mathrm{PA-ZnO}}(z) - [\rho_{\mathrm{PA-H}}(z) - \rho_{\mathrm{H}}(z)] - [\rho_{\mathrm{ZnO}}(z)] \quad (4)$$

Where PA-ZnO is the optimized, bidentate-bound system, PA-H is the molecule, removed from the surface in its bound geometry with the hydrogen atom that was lost upon surface binding re-attached, and ZnO is the prior surface with the SAM removed. The tridentate case is a bit more complex, but follows a similar method:

$$\Delta\rho(z) = \rho_{\mathrm{PA-ZnO-H3}}(z) - [\rho_{\mathrm{PA-H1-H2}}(z) - \rho_{\mathrm{H1}}(z) - \rho_{\mathrm{H2}}(z)] - [\rho_{\mathrm{ZnO-OH}}(z) - \rho_{\mathrm{H4-OH}}(z) + \rho_{\mathrm{H4}}(z)] - [\rho_{\mathrm{H5-H3}}(z) + \rho_{\mathrm{H5}}(z)] \quad (5)$$

In this case, PA-ZnO-H3 represents the optimized, tridentate-bound system with one hydrogen atom from the molecule (labeled H3) attached to the ZnO surface. PA-H1-H2 is the molecule, removed from the surface in its bound geometry, with both hydrogen atoms H1 and H2 re-attached. ZnO-OH corresponds to the bare surface, but with H3 replaced by the hydroxyl group originally lost by the chemisorption of the PA-SAM.

CHAPTER 3-

BINDING MOTIFS AND WORK FUNCTION MODIFICATION VIA FLUORINATED BENZYLPHOSPHONIC ACIDS

3.1 Introduction

Zinc Oxide (ZnO) is a transparent metal oxide that has gathered significant interest as electron-selective/electron-transport material for solar cells[53,54] and light-emitting diodes (LEDs)[55] and in sensor applications.[56] Chemical modification of the surface of metal oxides with small molecule adsorbates provides a method for tailoring the interface for optimal efficiency in each application.[57-59] Despite these advantages, there are only a few anchoring groups that have been studied; silanes,[60] amines,[61-63] thiols,[64-66] carboxylic acids,[67-73] and phosphonic acids.[74-76]

Phosphonic acids (PAs) have been used to successfully modify a variety of metal oxide materials.[77,78] They do not suffer from the same deposition and storage constraints as silanes necessitating the use of cross-linking techniques.[79,80] PA-modified ITO surfaces have been of recent interest for a variety of optoelectronic technologies,[81,82] and theoretical models have shown that PA monolayers can form in both bidentate and tridentate binding modes.[83] Recent work has shown that PAs can form stable monolayers on ITO in a bidentate-bound geometry, creating a more homogenous surface with a lower surface energy and better interfacial compatibility with deposited organic overlayers.[84] PAs have been used to modify ZnO nanoparticles,[85,86] and several reports detail the modification of planar ZnO substrates. For example, Sinapi *et al.* report on the modification of oxidized zinc substrates with alkylphosphonic acids, but they do not discuss the binding modes of the phosphonic acids to the substrate or the conformation of

the alkyl chains in the resulting monolayers.[87] A study by Perkins compares the use of hexylphosphonic acid and hexanethiol as surface modifiers for ZnO.[88] It was found that n-hexane derivatives of the phosphonic acid formed monolayers that provided both better corrosion resistance against Brønsted acids and thermal stability in comparison to monolayers formed from the thiol analog.

A series of fluorinated phosphonic acid SAMs chemisorbed to the zinc-terminated (0002) ZnO surface have been modeled in two different binding motifs. Binding energies have been calculated along with the 1s core-level binding shifts for the oxygen atoms in the PO_3 moiety with respect to the oxygen in the bulk zinc oxide, and these results are compared to experimental data.[75,76] The change in surface work function upon application of the SAMs has been determined, and the contributing terms have been individually calculated and compared between each system. As a result, a better understanding of the interacting factors that change the observed surface work function has been found, aiding in the design of phosphonic acid SAMs for future device applications.

3.2 Surface and Choice of Compounds

The theoretical model of the zinc-terminated polar (0002) ZnO surface used in this investigation consists of a 6.50 x 5.63 Å surface unit cell in a repeated slab configuration, separated by a vacuum space larger than 20 Å. A dipole sheet is introduced in the middle of the vacuum gap to compensate for the dipole moment created by the asymmetric nature of the slab, and the dangling oxygen bonds on the bottom of the slab were

saturated with a sheet of hydrogen atoms with a charge state of ½e. The slab consisted of six Zn-O layers with the lower three frozen into its previously optimized crystal structure and the other three layers, along with any surfaces adsorbates, were allowed to relax over the course of the geometry optimizations.

The chosen surface contained Zn and O surface vacancies and was passivated by the addition of two hydroxyl groups per unit cell corresponding to a packing density of 5.47 x 10^{14} molecules cm^{-2}, one located in a bridging position between two surface zinc atoms and the other filling the neighboring surface oxygen vacancy.[47] The PA monolayer is composed of one benzyl-PA molecule per unit cell, which corresponds to a packing density of 2.73×10^{14} molecules cm^{-2}.

We have investigated four benzylphosphonic acids with varying degrees of fluorination, including ortho-diflurobenzylphosphonic acid (o2FBPA), benzylphosphonic acid (BPA), *para*-fluorobenzylphosphonic acid (pFBPA), and pentafluorobenzylphosphonic acid (5FBPA). The molecular structures are shown in Figure 4.

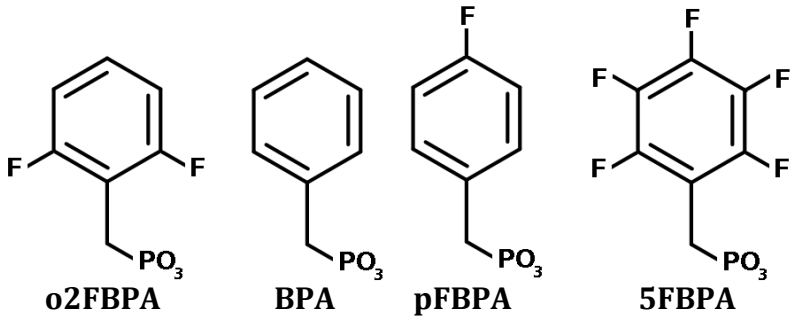

Figure 4. The four benzylphosphonic acids modeled in this chapter: ortho-diflurobenzylphosphonic acid (o2FBPA), benzylphosphonic acid (BPA), *para*-fluorobenzylphosphonic acid (pFBPA), and pentafluorobenzylphosphonic acid (5FBPA).

3.3 Binding modes

Several different binding modes have been proposed for PA[89] adsorption on transition metal oxide surfaces and are shown in Figure 5. The major adsorption modes are particularly sensitive to both the type of oxide surface and the surface treatment. For example, modes (a) (monodentate) and (b) (bidentate + electrostatic) have been suggested for PA adsorption on TiO_2,[90] Al_2O_3,[91,92] and $BaTiO_3$,[93] while tridentate mode (d) has been proposed to dominate on ZrO_2[94] and SiO_2.[89] Previous work in the group describing PA adsorption on ITO surface indicates that adsorption occurs via multiple modes, with a predominance of bidentate and tridentate modes (c) and (d), that involves P-O-In or P-O-Sn bonds.[83] Of these different possible binding modes, only two, (b) and (d) were found to be stationary points on the ZnO(0002) surface and chosen for a more detailed investigation. It is interesting to note that the bidentate binding mode shown in Figure 5(c) is not found in our calculations. Optimizations starting from this structure led directly to the tridentate mode.

The surface and a typical adsorbate are shown in Figure 6. To form the bidentate surface complex, one of the surface hydroxide groups has reacted with an acidic hydrogen in a dehydration reaction:

$$\mathrm{OH\text{-}ZnO} + \mathrm{RPO_3H_2} \rightarrow \mathrm{RPO_3H\text{-}ZnO} + \mathrm{H_2O}$$

The P-O double bond then binds to one of the under-coordinated zinc atoms on the surface. Thus, in the bidentate-bound mode, two of the PA oxygen atoms are bound to two zinc surface atoms and one acidic hydrogen still attached to the PA molecule forming

the monolayer. In the tridentate-bound case, the proton migrates to the surface, resulting in each of the three PA oxygen atoms becoming bound to a different surface zinc atom.

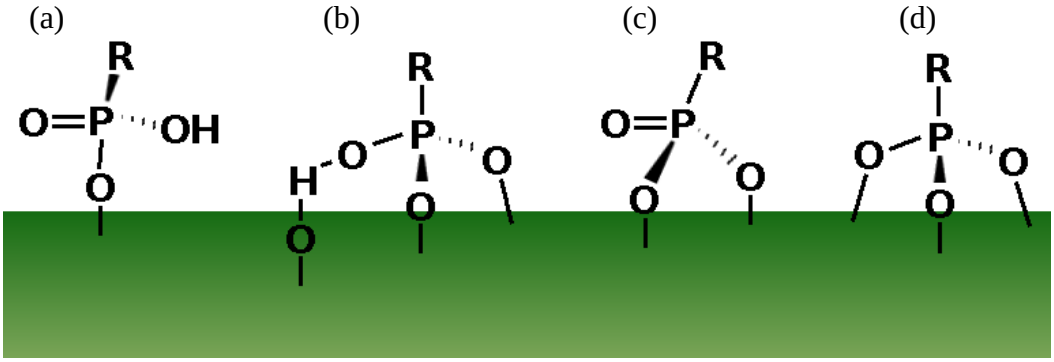

Figure 5. Potential metal oxide binding modes for organic phosphonic acids

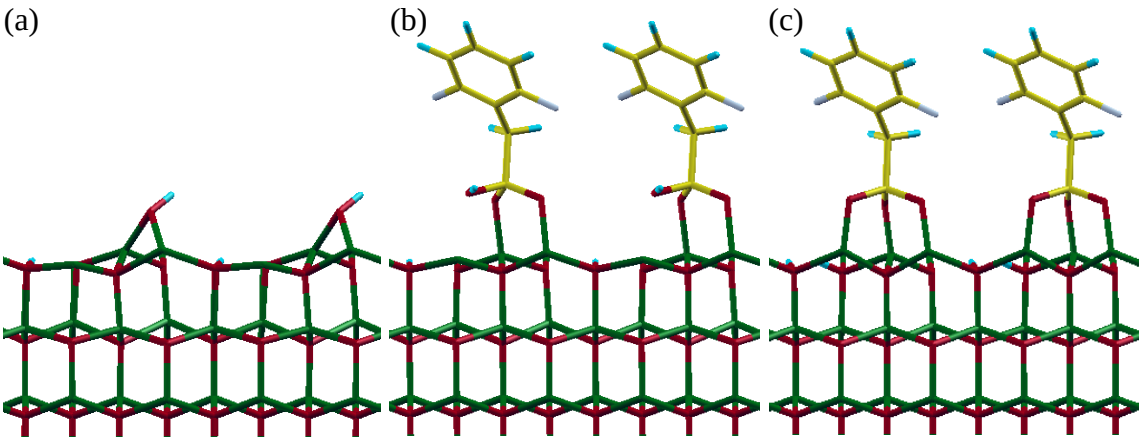

Figure 6. Side view of the initial ZnO(0002) surface (a), showing the two different binding geometries (shown using the di-fluorinated 2FBPA SAM) in the bidentate (b) and tridentate (c) binding mode.

3.4 Binding Geometries and Energies of Different Binding Motifs

The binding energies of both the bi- and tridentate-bound PA-SAMs are shown in Table 1. The binding energy is defined as the difference in total energy of the combined

surface and molecule before and after formation of the SAM; negative values correspond to an overall decrease in energy in the bound state corresponding to a thermodynamically-favored geometry. Each adsorption reaction is favorable with a total energy less than the sum of their unbound components, with the bi- and tridentate-bound PA-SAM having a binding energy of -1.5 eV and -2.1 eV respectively. The tridentate mode is approximately 0.6 eV lower in energy than its bidentate-bound counterpart. This is reasonable given the formation of an additional O-Zn bond. The binding geometries for each PA-SAM are similar: for the benzylphosphonic acid SAM in the tridentate binding mode, the angle of the benzyl ring relative to the oxide surface is 45.5°; the angle is 43.4° for the bidentate-bound SAM. Fluorination of the aromatic ring causes only minimal changes to this structure as the other SAMs range from 45.1° – 47.4° for the tridentate-bound mode and 43.4° – 47.2° for the bidentate-bound mode. This leads to only a minimal difference in the orientation of the ring relative to the surface.

The length of the bond between the benzyl carbon and the phosphorus (C-P) and its angle relative to the surface for each PA are also very similar: 1.82 (± < 0.01) Å and 80.4° – 81.1° for the tridentate-bound PA-SAMs and 1.83 (± < 0.01) Å and 81.2° – 82.4° for the bidentate-bound PA-SAMs. The average Zn-O bond lengths for the three tridentate-bound PA oxygen atoms are nearly constant, calculated at 1.856 (±0.001) Å for all four systems; by comparison, the Zn-O bond lengths for the bidentate-bound PA-SAMs average 1.985 (±0.002) Å, 0.13 Å longer than found in the tridentate-bound systems. These results are in agreement with the smaller calculated bidentate binding energy.

Table 1. Comparison of the binding energy and various surface angles and bond lengths for the various tridentate- and bidentate-bound PA-SAMs

		Angles (°)			Bond Lengths (Å)			
Bidentate	B.E. (eV)	Ben/ZnO	C-P/ZnO	P-O-Zn	C-P	P-O	PO-Zn	P-OH
o2FBPA	-1.53	46.0	81.2	120.4	1.836	1.553	1.983	3.748
BPA	-1.56	43.4	82.4	120.3	1.829	1.554	1.987	3.772
pFBPA	-1.54	44.1	82.5	120.2	1.828	1.554	1.988	3.769
5FBPA	-1.56	47.2	81.3	120.3	1.837	1.552	1.986	3.707
Average	-1.55	45.2	81.9	120.3	1.833	1.553	1.986	3.749
Tridentate								
o2FBPA	-2.12	46.2	80.6	117.4	1.826	1.855	1.983	-
BPA	-2.14	45.5	80.4	117.6	1.819	1.855	1.987	-
pFBPA	-2.13	45.1	81.1	117.6	1.820	1.856	1.988	-
5FBPA	-2.16	47.4	80.7	117.3	1.826	1.857	1.986	-
Average	-2.14	46.1	80.7	117.5	1.823	1.856	1.986	-

3.5 O(1s) Core-Level Binding Energy Shifts

Since the core-level electro0ns of the oxygen atoms in the phosphonic acid anchoring group are likely to be sensitive to their chemical environment, the 1s binding energy for the three PA oxygen atoms in each molecular SAM are calculated relative to the O(1s) core electrons in the bulk-like ZnO. For the energetically-favored tridentate binding mode, the calculated binding energy shift was +1.07 eV across all four systems. For the bidentate binding mode, the bound PA oxygen atoms had a calculated shift averaging 1.99 (± 0.03) eV and the unbound PA oxygen atom had a shift of 3.75 (± 0.03) eV. The 1.99 eV shift is coincidentally almost identical to the 1.98 eV shift calculated in our earlier work for a hydroxyl group bound to an oxygen vacancy site on the ZnO surface.[47] It is expected from these results that the XPS spectra of the modified ZnO surface by these PA-SAMs would generate a strong O(1s) peak shifted 1.07 eV from the dominant

ZnO peak, with two much weaker peaks corresponding to the bidentate-bound motif around +1.99 eV and +3.75 eV, with the 1.99 eV peak likely coinciding with the peak corresponding to the remaining hydroxyl groups on the surface. The surface oxygen species behave similarly in ZnO upon PA binding as they do in ITO. This can be compared to prior experimental work on polycrystalline ZnO, ZnO nanowires and sputter-deposited ZnO films.[75,76,88] The XPS of 1-hexanephosphonic acid on polycrystalline ZnO show the main O (1s) peak at 531.2 eV with an additional peak at 1.9 eV higher than the lattice peak attributed to surface hydroxyl groups. Upon addition of the SAM a third peak appears at +1.0 eV from the bulk peak. The O (1s) spectra of carboxyalkylphosphonic acid on ZnO nanowires was fit to five separate oxygen types. The bulk peak was found at 530.3 eV, with additional components at +1.1 and +1.8 eV from the phosphonic acid and two components at +2.6 and +3.5 eV from the unbound carboxylic acid. Spectra from the bulk carboxyalkylphosphonic acid show a peak from the P-OH at 532.3 eV and a peak from the P=O group at 531.2 eV. The binding mode of PAs on sputter-deposited ZnO follows the same pattern as the previous two experiments. A solvent-clean ZnO surface had an XPS O (1s) peak at 530.0 eV, which was attributed to the bulk oxygen species, and a shoulder at 531.6 eV associated with surface hydroxyl groups. Upon the binding of PAs, an additional peak at 531.0 eV (+1.0 eV) appeared, accompanied by a decrease in the intensity of the peak associated with surface hydroxyl groups, which was attributed to the formation of P–O–Zn bonds.

These observations, in combination with the calculated binding energies and O (1s) core level binding energy shifts, strongly suggest that the thermodynamically-favored tridentate-binding motifs are the component that has been largely observed in experiment.

However, the bidentate-bound geometry is still energetically favored over the unbound state and due to the chaotic nature of the polar ZnO surface it might be possible to find surface regions containing this binding mode.

Table 2. O(1s) core-level energy shifts ($\boldsymbol{E}_{\mathbf{SCLS}}$) in eV for each of the four PA-SAMs in both binding modes.

Molecule	Bidentate(P-O-H)	Bidentate	Tridentate
o2FBPA	3.75	1.98	1.07
BPA	3.77	2.01	1.07
pFBPA	3.77	2.02	1.07
5FBPA	3.71	1.94	1.07
Average	3.75	1.99	1.07

3.6 Electronic Density of States

As previously discussed, the conduction band minimum (CB_{min}) was used as the pseudo-Fermi-level for the calculation of the work function Φ to compare with the experimental measurements on the unintentionally n-type doped ZnO. A decomposition of the charge density associated with CB_{min} and VB_{max} was performed for each system and shown in Figure 7. For both the bi- and tridentate bound systems, the CB_{min} is located predominantly within the bulk of the ZnO, indicating that the CB_{min} of the ZnO surface is not affected by the surface modification via the PA-SAMs. This also confirms that the use of CB_{min} as the pseudo-Fermi-level is valid for the PA-ZnO complex. However, a significant difference has been observed in the VB_{max} for the two different binding geometries. In the bidentate system, this is predominately the O(2p) orbitals within the top two Zn-O layers, while for the tridentate-bound systems this corresponds to the

contribution of the molecular SAM. A partial density of states (PDOS) plot for the different atoms was generated for each system; an example is presented in Figure 8. The PDOS projected to the F and C atoms in the PA molecule shows that the energy level of the highest occupied molecular orbital (HOMO) of the tridentate-bound PA-SAM is aligned with the top of the ZnO valence band, which is consistent with the charge distribution shown in Figure 6(b). For the bidentate-bound o2FBPA-SAM, its HOMO level is 1.8 eV below the VB_{max} of the ZnO surface. These results show that the binding mode has a significant effect on the energy level alignments of the molecular frontier orbitals with respect to the band edges of the metal-oxide semiconductor.

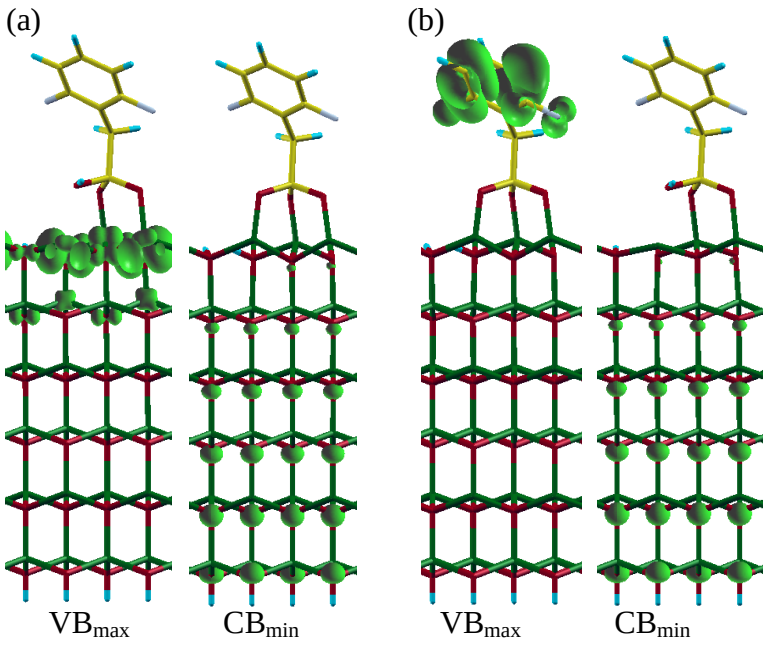

Figure 7. Depiction of VB_{max} and CB_{min} both the bi- (a) and tridentate-bound (b) 2FBPA system

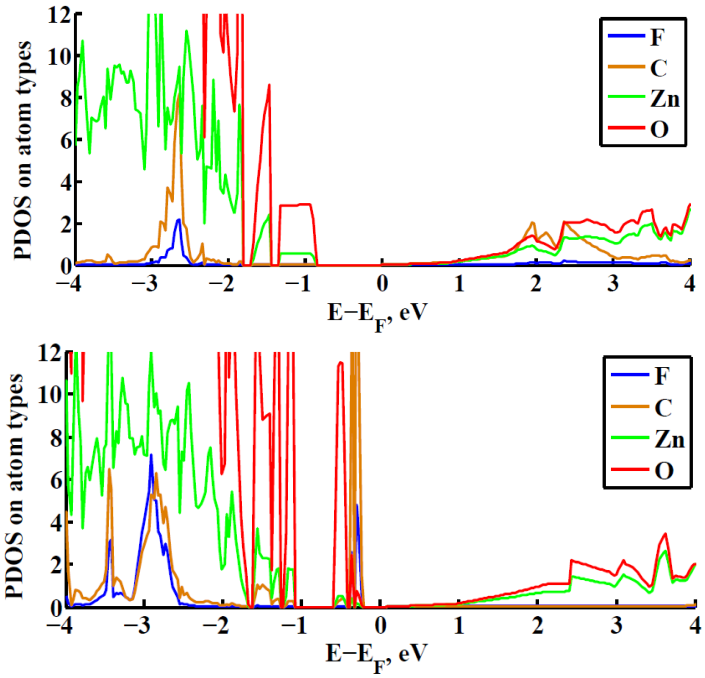

Figure 8. Density of states for both the bi- (a) and tridentate (b) bound 2FBPA system

3.7 Change in Work Function

The work function of the bare ZnO surface model adopted in this work is calculated to be 4.43 eV, which is consistent with the experimental values varying from 3.5-4.3 eV. [52,95] The change of work function for each PA-modified ZnO surface is calculated and given in Table 3. The range in work function modifications for different fluorination patterns is more than 1.5 eV for the bidentate case, and in the tridentate case the range is 1.3 eV. This is the same range as in previous studies using semifluorinated alkanethiols on gold surfaces[96] and fluorinated benzylphosphonic acids on ITO surface.[97,98]

As in our previous work on the PA-modified ITO surface, a correlation between the component of the molecular dipole moment perpendicular to the surface and changes in surface work function has been observed. It can be clearly seen that the SAMs are

ordered by increasing relative strength of electron-withdrawing ability: 5FBPA has the largest increase of Φ with ΔΦ= +2.14 eV and o2FBPA has the smallest with ΔΦ = +0.89 eV. For each PA modifier, we also considered an isolated monolayer with the same geometry as adsorbed on the ZnO surface, in order to evaluate the component of the dipole moment (μ_z) perpendicular to the surface. Plotting $\mu_{z(SAM)}$ against the calculated change in work function (ΔΦ) shows a linear trend (see Figure 9 and Table 3). The bidentate-bound data set shows a similar linear trend to the tridentate SAMs. However, the entire data set is shifted downwards: the bidentate-bound systems have ΔΦ values that are 2.1-2.3 eV lower than those found in the equivalent tridentate-bound system. The difference in the dipole moment normal to the surface for the different binding modes must be a function of the change in bonding in the phosphonic acid anchor group, since the relative orientation of the phenyl group is nearly constant (as seen in Table 1). The intercept of this line indicates that, when the molecular dipole moment is zero, the intrinsic shift in effective work function for the bidentate configuration is -0.29 eV and for the tridentate configuration is 1.56 eV. There is a slightly stronger correlation in the bidentate-bound mode than in the tridentate-bound mode; however the difference in both the slope and the intercept of the linear fit indicate that there are additional factors involved.

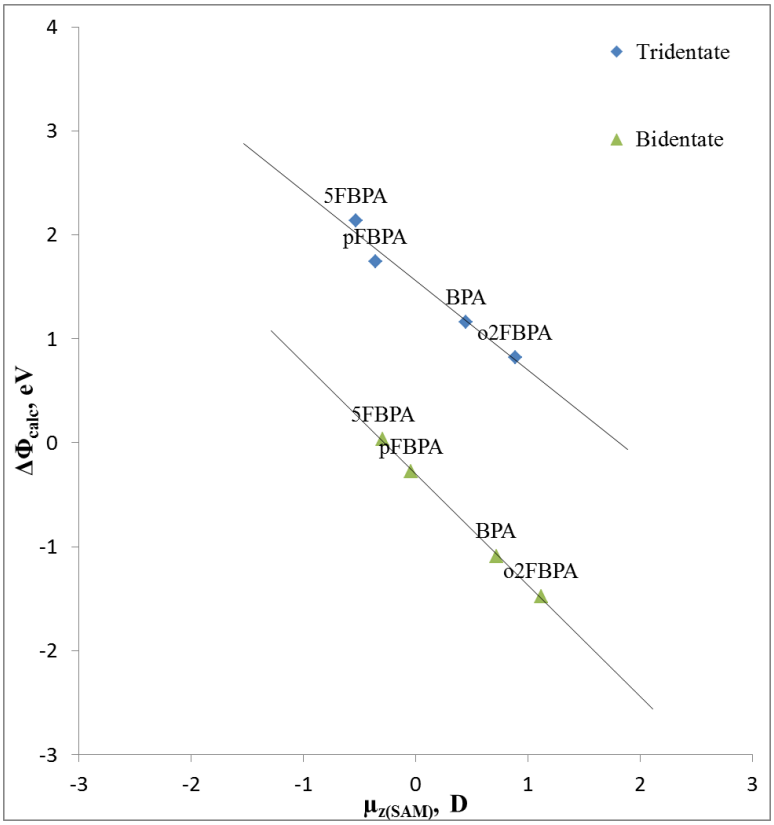

Figure 9. Relationship of ΔΦ compared to $\mu_{z(SAM)}$.

Table 3. ΔΦ and $\mu_{z(SAM)}$ values for the bi- (left) and tridentate-bound (right) SAMs used in Figure 9.

	$\mu_{z(SAM)}$ (D)	ΔΦ (eV)		$\mu_{z(SAM)}$ (D)	ΔΦ (eV)
o2FBPA	+ 1.12	- 1.48	o2FBPA	+ 0.89	+ 0.82
BPA	+ 0.72	- 1.09	BPA	+ 0.45	+ 1.16
pFBPA	- 0.04	- 0.28	pFBPA	- 0.36	+ 1.74
5FPBA	- 0.29	+ 0.03	5FPBA	- 0.53	+ 2.14

3.8 Decomposition of the Work Function

As discussed earlier, the change in work function can be decomposed into three components: the bond dipole due to the charge-redistribution at the interface of the SAM and the surface (BD), the change in the potential energy crossing an isolated molecular SAM (ΔV_{vac}), and the change in work function due to the geometry reorganization of the surface upon application of the SAM ($\Delta\Phi_{geo}$). Each of these terms is calculated separately, tabulated in Table 4, and depicted in Figure 11. This is a change from the case of fluorinated benzylphosphonic acids on ITO where the term dealing with the geometric change of the surface was omitted due to the low packing density of the surface modifiers.[97] This term was found to be important as the coverage density increased.[98] The values for the change in work function, $\Delta\Phi_{tot}$, are consistent compared to the calculated values for $\Delta\Phi$ using the DFT-derived potential for the combined system. For the tridentate-bound SAMs, there is an overestimation of the work function by 0.1 eV while for the bidentate-bound SAMs, there is an underestimation of 0.1 eV.

Values for ΔV_{vac} are related to $\mu_{z(SAM)}$, which was shown to be the principal component in the variation of $\Delta\Phi$ (although only one contributing component of $\Delta\Phi$), through the Helmholtz equation. The values for $\Delta\Phi_{geo}$ are very similar for each SAM, with the bidentate-bound mode showing an average shift of -1.45 eV, 0.6 eV larger than the -0.87 average downward shift in $\Delta\Phi_{geo}$ seen in the tridentate binding mode. The overall similarity within each binding mode is as expected due to the very similar geometries of each system; as a result, although this geometric shift is an important contributor to $\Delta\Phi$, it has little impact on any attempt to tune the overall surface work function change by modifying the PA monolayer.

The final contributing factor, the bond dipole, has a much more significant level of variance for the tridentate-bound SAMs (0.35 eV) when compared to the bidentate-bound SAMs (0.06 eV), and provides the remaining contribution to the variance in $\Delta\Phi$ found in the tridentate-bound molecular SAM. The level of variation in the bond dipole is significantly greater than in the case of benzylphosphonic acids on ITO. It was expected that the lack of significant differences between the optimized geometries for each system would result in no significant variance observed in the bond dipole, but calculations have demonstrated that the bond dipole is extremely sensitive to variations in the aryl electronic structure. This indicates that there is a stronger interaction between the aryl head-group and the phosphonic acid docking-group for the tridentate bound systems than those in the bidentate binding motif. This stronger interaction can be clearly seen by comparing the charge transfer from the ZnO surface to the molecules for the two different binding modes (Figure 11). In the tridentate binding case (Figure 11b), an accumulated charge of about 0.5e is transferred from the ZnO surface to the PO_3 moiety of the molecule; whereas an accumulated charge of about 0.2e is transferred from the ZnO surface to the molecule in the bidentate binding motif (Figure 11a). The significant difference in charge transfer also explains the large shift in bond dipole for the two binding motifs.

Table 4. Decomposition of the work function into its contributing factors: the molecular vacuum shift, the work function change due to surface geometry reorganization, and the bond dipole (all values in eV).

Bidentate

	ΔV_{vac}	$\Delta\Phi_{geo}$	BD	$\Delta\Phi_{tot}$
o2FBPA	-1.15	-1.48	1.23	-1.38
BPA	-0.75	-1.45	1.20	-1.00
pFBPA	0.04	-1.46	1.17	-0.24
5FBPA	0.30	-1.42	1.21	0.08

Tridentate

	ΔV_{vac}	$\Delta\Phi_{geo}$	BD	$\Delta\Phi_{tot}$
o2FBPA	-0.91	-0.87	2.47	0.69
BPA	-0.46	-0.88	2.40	1.05
pFBPA	0.36	-0.86	2.12	1.62
5FBPA	0.54	-0.82	2.27	2.00

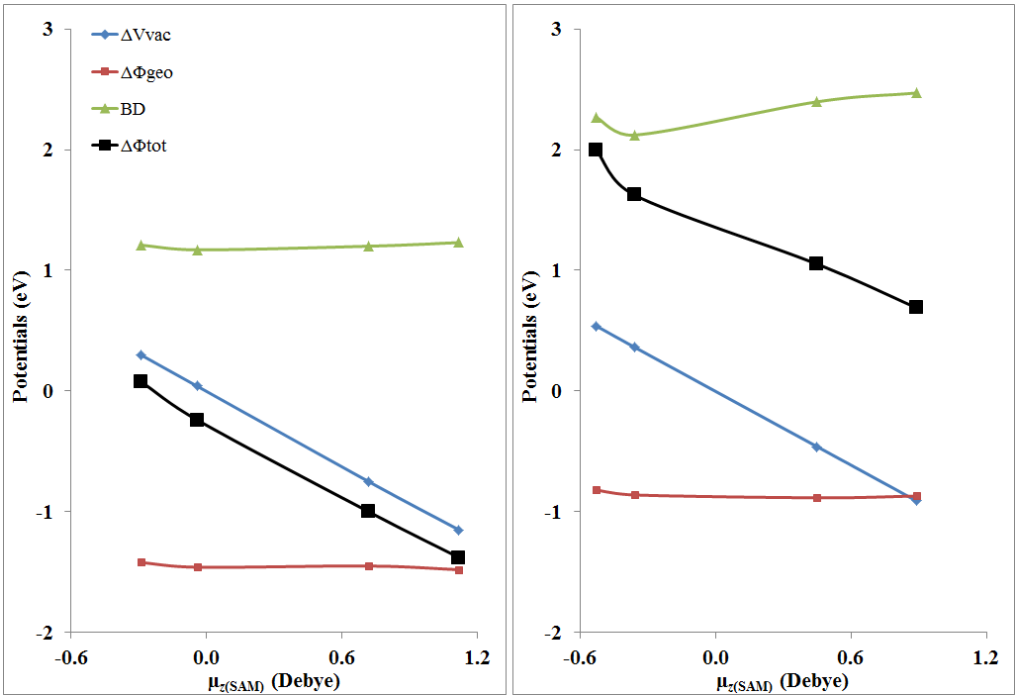

Figure 10. Relationship of the decomposed components of the change in work function (ΔV, $\Delta\Phi_{geo}$, and the bond dipole) and the total of these three components ($\Delta\Phi_{tot}$) compared to $\mu_{z(SAM)}$ for both the bi- (a) and tridentate-bound (b) SAMs.

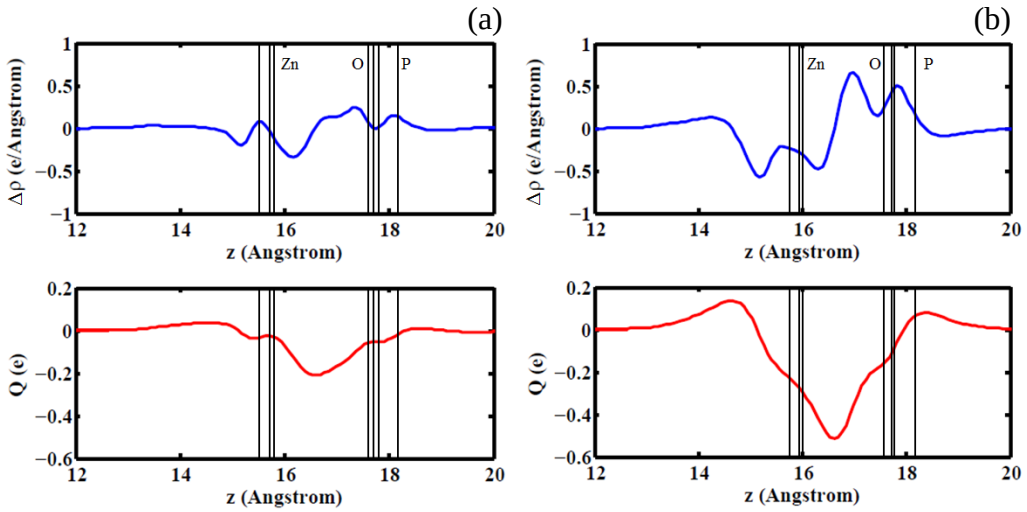

Figure 11. A comparison of the change in electron density (Δρ) and accumulation of Δρ (Q) upon formation of the SAM for both the bi- (a) and tridentate-bound (b) SAMs.

3.9 Conclusion

The binding energies, O(1s) core level binding energy shifts of the PO_3 moiety with respect to the oxygen in bulk-like ZnO, electronic density of states, changes in work function, and their contributing components have been calculated using density functional theory for a series of four benzylphosphonic acid SAMs with varying degrees of fluorination deposited on the polar (0002) ZnO surface. The tridentate binding mode was found to be 0.6 eV more thermodynamically favored than the bidentate binding mode. Although the two binding modes each show little difference in terms of molecular orientation and surface binding geometry, it has been found that they have a significant impact on the energy level alignments of the molecular HOMO relative to the valence band maximum of ZnO. The overall shifts in work function show that the predominant tridentate-bound molecular SAMs caused an overall increase in work function for all four benzylphosphonic acids, while the weaker-bound bidentate mode could lead to reductions

in work function- except for the pentaflurobenzylphosphonic acid SAM. It is interesting that the bond dipole term is the largest in magnitude for the substitutions studied here. Finally, the various tridentate-bound SAMs were shown to have a much larger variance in their respective bond dipoles, relating to a larger effect of molecular substitutions on the charge-redistribution at the interface of stronger, tridentate-bound SAM on the ZnO substrate. Thus we have provided a detailed and systematic study of the modification of a polar ZnO surface via phosphonic acids. This level of detail is critical in understanding the observed change in work function as details of the deposition process and resulting surface coverage can possibly lead to differing binding modes.

CHAPTER 4-

SURFACE MODIFICATION VIA SUBSTITUTED BENZYL- AND PHENYL PHOSPHONIC ACIDS

4.1 Introduction

In earlier works on the SAMs of π-conjugated molecules formed on noble metals,[99] the docking group, where the monolayer attached to the surface, and the headgroup, the portion of the SAM exposed to the region above the surface, have been seen to act independently in tuning the work function. For example, on a gold substrate there was only a 0.03 eV change in the bond dipole term for phenylthiol salts, which captures the interfacial charge rearrangement due to bonding, when varying the headgroup between amino, thiol and cyano moieties and maintaining the thiol docking group. On ITO, fluorination of benzylphosphonic and phenylphosphonic acids led to only minor changes in the bond dipole term. These results are somewhat surprising given that reactivity of aromatic compounds is generally dictated by the nature and relative position of functional groups attached to the ring.

In contrast to these results, the prior chapter on fluorinated benzylphosphonic acids indicated that there was significant change in the bond dipole for tridentate-bound species on ZnO(0002). It was expected that the lack of significant differences between the optimized geometries for each system would result in no significant variance observed in the bond dipole as was seen previously, but calculations have demonstrated that the bond dipole is extremely sensitive to variations in the aryl electronic structure. In order to understand the influence of π-active substituents on the surface modification of oxide surfaces, we present a study of various *para*-substituted benzyl- and phenyl-phosphonic

acid self-assembled monolayers (PA-SAMs) on the polar(0002) ZnO surface. The change in surface work function upon deposition of the SAMs has been determined, and the contributing terms have been individually calculated and compared between each system. The relationship between the gas-phase molecular dipole and the molecular dipoles of each SAM normal to the surface have also been studied: as the primary contributor to the variance in $\Delta\Phi$ with respect to the choice of molecular SAM, a better understanding of this relationship and its contributions to the observed surface work function will prove very useful.

4.2 Binding Motifs and Choice of Compounds

We have investigated benzyl- and phenylphosphonic acids with a diverse set of both electron donating (*e.g.*, $-N(CH_3)_2$, $-OCH_3$, -SH, $-CH_3$) and electron withdrawing (*e.g.*, -F, $-NO_2$) substituents on the *para*- position. The basic structure of these molecules is displayed in Figure 11. In the previous chapter, the tridentate binding mode was found to be approximately 0.6 eV more thermodynamically favored than the bidentate binding mode for all of the benzylphosphonic acids in the study; thus, we have used the tridentate mode in these calculations with a packing density of 2.73×10^{14} molecules cm^{-2}.

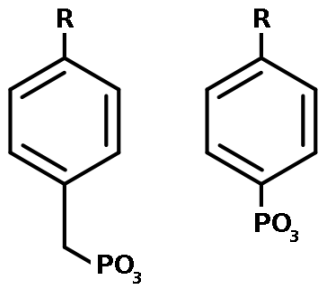

Figure 12. The basic structure of the *para*-substituted phosphonic acids (PAs) used in this study. R= NMe_2, OMe, CH_3, H, SH, F, and NO_2.

4.3 Binding Geometries and Binding Energy

The binding geometries for each PA monolayer are similar (see Figure 13 and Table 5); for the unsubstituted benzyl- and phenyl-PAs the angle of the aromatic ring relative to the oxide surface is 43.7° and 82.9°, respectively. The surface angles for the substituted benzyl-PAs range from 43.7° – 46.5° and from 81.7° – 88.1° for the various phenyl-PAs. From this data, it is evident that the additional CH_2 in the benzyl-PAs results in a much smaller angle relative to the surface, which is only modified slightly by the bulkier *para*-substitutions in the various densely-packed monolayers. The length of the P-C bond and its angle relative to the surface for each PA are also similar: 1.82 (± < 0.01) Å and 80.1° – 81.9° the benzyl-PAs, and 1.79 (± < 0.01) Å and 85.9° – 87.4° for the phenyl-PAs. The average Zn-O bond lengths for the three tridentate-bound PA oxygen atoms are highly consistent, calculated at 1.86 (± < 0.01) Å for all fourteen systems.

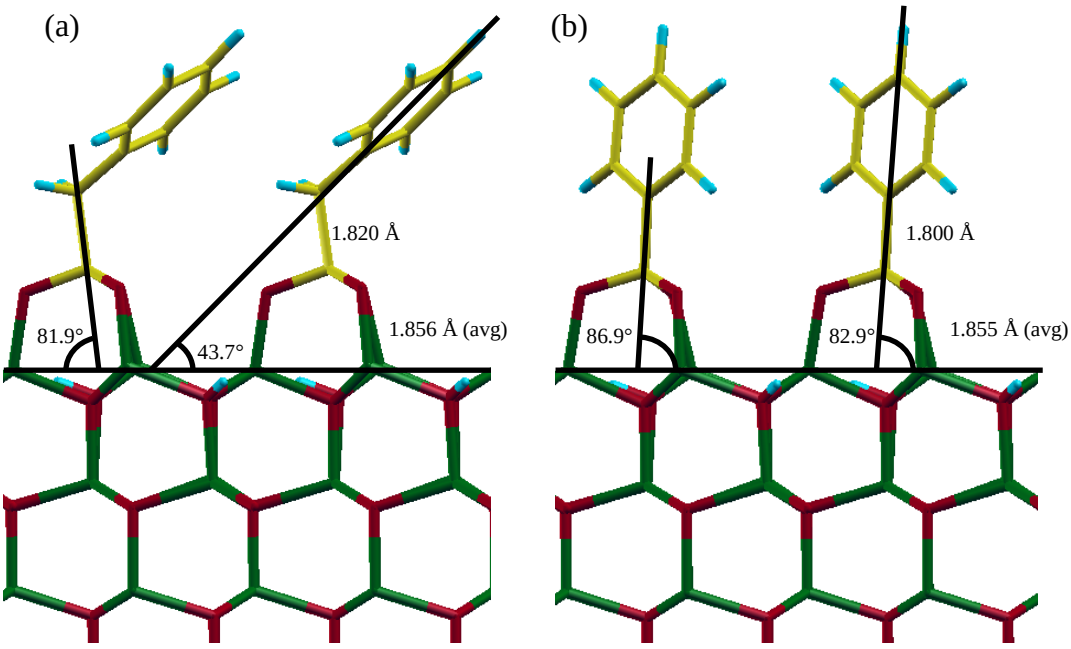

Figure 13. Side view of the ZnO(0002) surface with (a) benzyl PA and (b) phenyl PA showing the surface angles, C-P bond distances, and average Zn-O bond distances.

Table 5. Comparison of the various surface angles and bond lengths for the various PA monolayers

	Benzyl				**Phenyl**			
	Surface Angles (°)		Bond Lengths (Å)		Surface Angles (°)		Bond Lengths (Å)	
R=	Ben/ZnO	C-P/ZnO	C-P	O-Zn	Ben/ZnO	C-P/ZnO	C-P	O-Zn
NMe_2	45.4	80.1	1.825	1.861	88.1	86.0	1.794	1.857
OMe	44.6	80.5	1.821	1.856	84.8	87.4	1.794	1.853
CH_3	45.5	80.4	1.819	1.855	83.7	86.0	1.795	1.853
H	43.7	81.9	1.820	1.856	82.9	86.9	1.800	1.855
SH	46.5	80.9	1.823	1.859	82.6	86.4	1.795	1.854
F	45.1	81.1	1.820	1.856	81.7	85.9	1.796	1.854
NO_2	45.2	80.5	1.822	1.857	83.8	86.4	1.801	1.856

While a consistent coverage density was used for each SAM, this work considers both phenyl- and benzyl-PAs, and the intermolecular distances between the molecules in the monolayers are not constant. For the benzyl-PAs, the shortest intermolecular distance is

between a benzyl hydrogen and a ring hydrogen on an adjacent molecule, with an average center-to-center distance of 3.18 Å (see Figure 13). In contrast, for the phenyl-PAs, the shortest distance is measured between phenyl hydrogen atoms on adjacent molecules, averaging a distance of 4.26 Å. Taking into account the van der Waals radius of hydrogen, the resulting minimum distance between molecules becomes 0.78 Å and 1.86 Å, respectively.

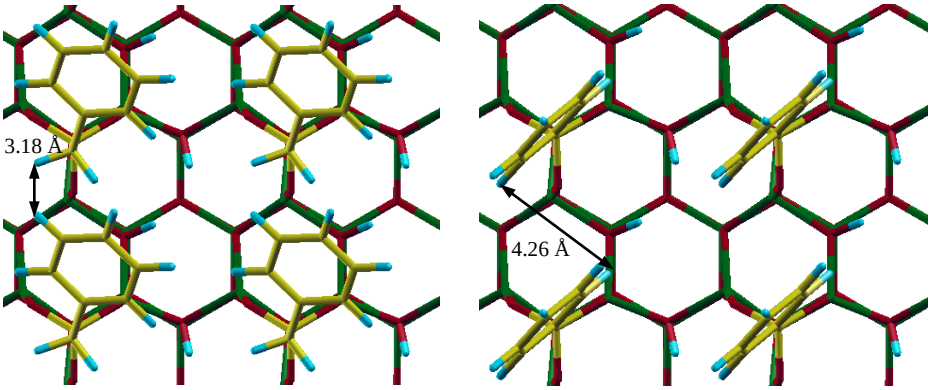

Figure 14. Comparison of the minimum distance between molecules for the benzyl PA (left) and the phenyl PA (right)

The calculated binding energies for each SAM, shown in Table 6, are nearly constant, with the benzyl-PAs having slightly weaker (< 0.1 eV) binding energies than the analogous phenyl-PAs. This could be partially attributed to the weak repulsions between hydrogens on adjacent molecules in the SAM. There was little variation in binding energy with respect to substitution as the phenyl-PAs ranged from -2.14 to -2.24 eV and the benzyl-PAs ranged from -2.10 to -2.17 eV. For both sets of phosphonic acids the strong electron-donating dimethylamine and the strong electron-withdrawing nitro substituents were the weakest-bound complexes.

Table 6. Comparison of the binding energy for the substituted benzyl- and phenyl- PAs

	Binding Energy (eV)	
R=	Benzyl	Phenyl
NMe_2	-2.12	-2.14
OMe	-2.14	-2.21
CH_3	-2.14	-2.20
H	-2.15	-2.21
SH	-2.16	-2.24
F	-2.13	-2.21
NO_2	-2.10	-2.14

4.4 Change in Work Function and Molecular Dipole

The calculated change of work function for each PA-modified ZnO surface is given in Table 7. The electron-rich substituents result in a decrease in the work function while the electron-deficient groups result in an increase; for example, the dimethylamino benzyl- and phenyl-phosphonic acids have a decrease in work function of -1.01 and -1.03 eV, respectively. The nitro-substituted benzyl- and phenyl-PAs have the largest increase, with increases of 3.13 and 3.68 eV. The range in work function modifications for different substitutions is nearly 4 eV. This is significantly greater than the range in work function modifications that have been seen previously, although this can be partially attributed to the much higher molecular packing density compared to earlier works.[100]

Table 7. Changes in work function for the various benzyl- and phenyl-PA SAMs

	$\Delta\Phi_{calc}$ (eV)	
R=	Benzyl	Phenyl
NMe_2	-0.87	-1.02
OMe	0.30	0.27
CH_3	0.79	0.68
SH	0.83	0.77
H	1.16	1.00
F	1.74	2.11
NO_2	3.29	3.68

As in the previous chapter, a correlation has been observed between the component of the molecular dipole moment perpendicular to the surface and changes in the surface work function. Plotting $\mu_{z(SAM)}$ against the calculated change in work function ($\Delta\Phi$) shows a definite trend as seen in Figure 15. Given the diversity of substituents, the correlation is relatively high ($R^2 = 0.93$).

By comparing the molecular dipole moment perpendicular to the surface to the molecular dipole calculated for the molecules in the gas phase, an understanding of the influence of surface packing within the SAM can be gained. The component of the molecular dipole along the carbon-phosphorus bond, $\mu_{P\text{-}C}$, and the molecular dipole for each SAM projected normal to the surface, $\mu_{z(SAM)}$, can be seen in Table 8. In general, the influence of a substituent on $\mu_{P\text{-}C}$ for the phenyl-PAs is larger than those for benzyl-PAs as the benzene ring is aligned with the P-C bond. A linear regression of these terms suggests that the dipole moment of the benzyl molecule is reduced by a factor of 1.6 compared to its phenyl analog, which is approximately the ratio of the cosines that the aromatic rings make relative to the P-C bond.

Table 8. Comparison of the total gas-phase molecular dipole along the P-C bond and the dipole normal to the surface when in the SAM configuration for both the benzyl- and phenyl-PAs

	Benzyl			**Phenyl**	
	Gas	SAM		Gas	SAM
R=	μ_{P-C}	μ_z	R=	μ_{P-C}	μ_z
NMe_2	1.87	1.41	NMe_2	4.55	2.02
OMe	0.71	0.80	OMe	2.11	1.18
CH_3	1.00	0.61	CH_3	1.84	1.01
SH	0.13	0.02	SH	0.91	0.37
H	0.63	0.45	H	1.19	0.76
F	-0.52	-0.36	F	-0.43	-0.39
NO_2	-3.22	-1.80	NO_2	-4.11	-2.38

When comparing μ_{P-C} to $\mu_{z(SAM)}$, the value of the dipole is reduced by a factor of 0.52 and 0.59 for the benzyl- and phenyl-PAs, respectively. This reduction shows that there is a significant depolarization in both SAMs with the effect being greater in the benzylphosphonic acids. When making a direct comparison between the two values, there is only a small correction due to the fact that the carbon-phosphorus bond in the bound SAMs is not normal to the surface as it averages 86.5° for phenyl-PAs and 80.8° for benzyl-PAs. When comparing $\mu_{z(SAM)}$ for the phenyl- and benzyl-PAs, there is a reduction in the dipole moment perpendicular to the surface by a factor of 1.4. This is a due to the perpendicular nature of the phenyl-PAs, where the angle of the aromatic ring relative to the surface averages 83.9° compared to 43° for the benzyl-PAs, and the increased depolarization of the benzyl-PAs in comparison to the phenyl-PAs.

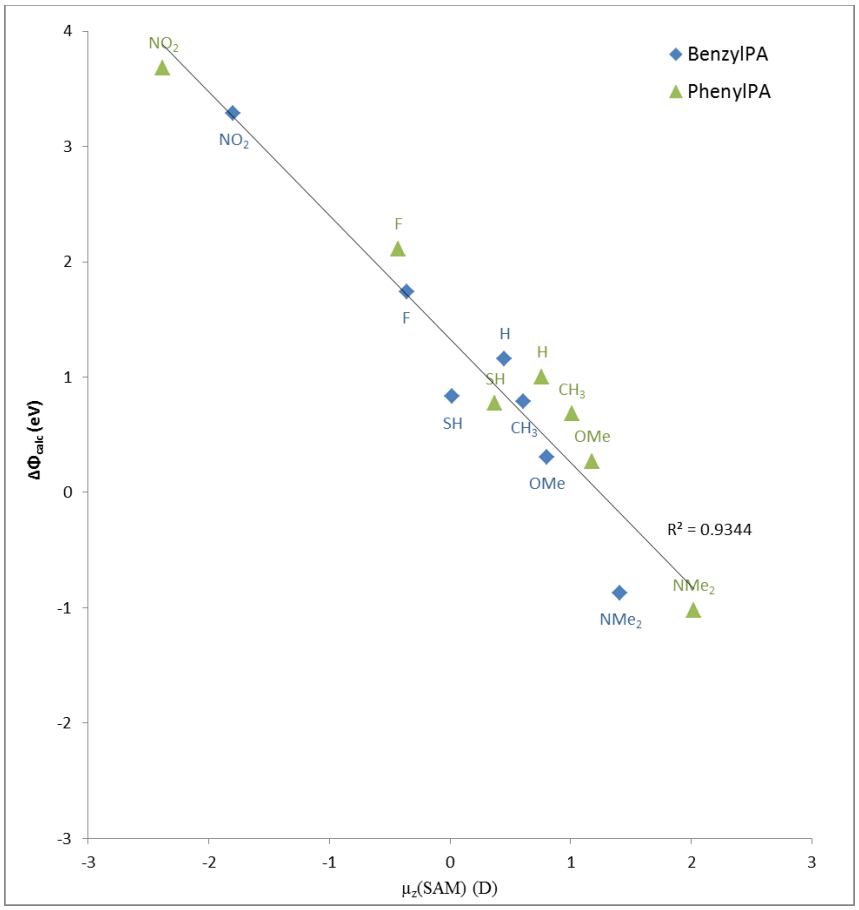

Figure 15. A plot depicting the calculated change in work function $\Delta\Phi_{calc}$ compared to the molecular dipole normal to the ZnO surface of each SAM. Benzyl-PA-SAMs are marked with blue diamonds, phenyl-PA-SAMs are marked with green triangles.

4.5 Decomposition of the Work Function

As discussed earlier, the change in work function can be decomposed into three components: the bond dipole due to the charge-redistribution at the interface of the SAM and the surface (BD), the change in the potential energy crossing an isolated molecular SAM (ΔV_{vac}), and the change in work function due to the geometry reorganization of the surface upon application of the SAM ($\Delta\Phi_{geo}$). Each of these terms are calculated separately and tabulated in Table 9. Values for ΔV_{vac} are related to $\mu_{z(SAM)}$, which was

shown to be the principal component in the variation of ΔΦ (although only one contributing component of ΔΦ), through the Helmholtz equation. The values for $\Delta\Phi_{geo}$ are very similar for each SAM, which was expected as the binding energies and the binding geometries are consistent for the substituents studied. This term is smallest for the dimethylamine substituted PA-SAMs, where it is 0.07 eV smaller than the phenyl-PA and 0.22 eV smaller than the benzyl-PA. There is no clear trend in $\Delta\Phi_{geo}$ for the other substitutions. The final contributing factor, the bond dipole, has a large degree of variance and provides the remaining contributions to ΔΦ.

Table 9. Decomposition of the work function for the benzyl- and phenyl-PAs into their contributing factors (all values in eV).

	Benzyl					**Phenyl**				
R=	ΔV	$\Delta\Phi_{geo}$	BD	$\Delta\Phi_{tot}$	$\Delta\Phi_{calc}$	ΔV	$\Delta\Phi_{geo}$	BD	$\Delta\Phi_{tot}$	$\Delta\Phi_{calc}$
NMe_2	-1.45	-0.66	1.09	-1.01	-0.87	-2.07	-0.84	1.88	-1.03	-1.02
OMe	-0.83	-0.78	1.79	0.18	0.30	-1.22	-0.96	2.40	0.22	0.27
CH_3	-0.63	-0.86	2.15	0.65	0.79	-1.03	-0.94	2.59	0.62	0.68
SH	-0.02	-0.79	1.50	0.69	0.83	-0.78	-0.92	2.64	0.74	0.77
H	-0.46	-0.88	2.40	1.05	1.16	-0.38	-0.91	2.03	0.94	1.00
F	0.36	-0.86	2.12	1.62	1.74	0.43	-0.92	2.53	2.05	2.11
NO_2	1.85	-0.83	2.11	3.13	3.29	2.45	-0.86	2.08	3.66	3.68

As was the case with the tridentate-bound systems in the prior chapter, the BD values calculated for both the benzyl- and phenyl- SAMs occur over a range of approximately 1 eV. This level of variation in the bond dipole is significantly greater than in the case of benzylphosphonic acids on ITO and ZnO, where the variations are 0.03 eV and 0.20 eV. This variation demonstrates that the bond dipole is extremely sensitive to either the small differences in the geometry at the surface-SAM interface or the aryl electronic structure;

The summed values for $\Delta\Phi_{tot}$ are consistent with the independently-calculated values for $\Delta\Phi$; for the phenyl-PA-SAMs, this difference is ~0.05 eV. For the benzyl-PA SAMs, there is a slightly larger (but still consistent) discrepancy ranging 0.11-0.16 eV lower than $\Delta\Phi$.

4.6 Conclusion

The binding geometries, binding energies, changes in work function, and their contributing components have been calculated using density functional theory for a series of fourteen *para*-substituted benzyl- and phenyl-phosphonic acid SAMs on the polar (0002) ZnO surface in the tridentate binding mode. The overall shifts in work function show that there continues to be a strong correlation between the molecular dipole of the SAMs, relating to their relative electron donating or withdrawing strengths and the overall increase in work function. The resulting difference in the work function change for a benzyl- and phenyl-PA with a given *para*-substitution respective is due primarily to the change in tilt angle of the aryl ring relative to the surface, which proved to be consistent across all cases; the phosphorus atom in the PO_3 group effectively shields the headgroup from the O-Zn bonds created upon formation of the monolayer. This work has provided a more detailed study of the tridentate modification of a polar ZnO surface via a larger selection of phosphonic acids.

CHAPTER 5-

FUTURE CONSIDERATIONS

A detailed investigation of a series of aryl-containing phosphonic acids on a single zinc- and oxygen-depleted, hydroxyl-modified, polar (0002) ZnO surface in two different binding modes has been described. However, there are a number of additional areas for future investigation; the zinc oxide surface is an unstable one, capable of containing a wide variety of surface defects. To better understand this surface, an expanded unit cell makes for a very obvious next step.

Modeling a larger unit cell would still be possible via the DFT techniques used in this study; a four-fold increase in cell size would create a system with ~200 atoms describing the surface. With starting geometries provided by the calculations performed with the smaller unit cell, modeling at least a small subset of the systems examined in this study would be computationally viable. By expanding the unit cell to a larger size, the effect of surface defects—in combination with the variance of PA coverage density—could be studied in much more detail. Recent discussions have revealed that despite the small (<0.1 eV) differences in binding energy calculated for the various molecules studied in this work, experimental observations have shown that there are dramatic differences in observed coverage densities for these molecules by as much as an order of magnitude. In addition, a larger unit cell could be used to investigate the existence of other possible thermodynamically-favored binding modes such as a bridged monodentate geometry: something that was not possible to model with the original unit cell containing a single molecule.

In addition, the small impact on binding energy observed by modifying the aryl component is likely due to the PO_3 phosphorus atom acting as a barrier preventing the modified head groups from altering the oxygen-zinc surface binding. A study of the 2p binding energy shifts for the phosphorus would be a useful next step for further investigation into this phenomenon. Further study into the exact position of the HOMO/LUMO levels of the carbon ring relative to the valence and conduction bands of the modified ZnO surface could also lead to a better understanding of the changes in the work function for these systems.

Finally, the energy barrier between the different binding modes is also of considerable interest; if this barrier is fairly low (with respect to kT) then it may be difficult to resolve specific binding modes from experimental data. More importantly, the variety of binding motifs would have a significant impact on the macroscopic electronic effect of SAM modification.

A solid understanding of how to modify the bond dipole, combined with the understanding of the relationships between molecular dipole and work function and the potential binding geometries outlined in prior chapters, would allow for a more accurate method for tuning the work function of metal oxide surfaces like ZnO using robust monolayers formed from custom-designed phosphonic acids for applications in a variety of organic electronic devices.

REFERENCES

(1) Newman, C. R.; Frisbie, C. D.; da Silva Filho, D. A.; Brédas, J.-L.; Ewbank, P. C.; Mann, K. R. *Chem. Mater.* **2004**, *16*, 4436.

(2) Facchetti, A.; Letizia, J.; Yoon, M.-H.; Mushrush, M.; Katz, H. E.; Marks, T. J. *Chem. Mater.* **2004**, *16*, 4715.

(3) Crone, B.; Dodabalapur, A.; Lin, Y. Y.; Filas, R. W.; Bao, Z.; LaDuca, A.; Sarpeshkar, R.; Katz, H. E.; Li, W. *Nature* **2000**, *403*, 521.

(4) Anthony, J. E. *Chem. Rev.* **2006**, *106*, 5028.

(5) Anthony, J. E. *Angew. Chem. Int. Ed. Engl.* **2008**, *47*, 452.

(6) Sirringhaus, H. *Adv. Mater.* **2005**, *17*, 2411.

(7) Sirringhaus, H.; Kawase, T.; Friend, R. H.; Shimoda, T.; Inbasekaran, M.; Wu, W.; Woo, E. P. *Science* **2000**, *290*, 2123.

(8) Friend, R. H.; Gymer, R. W.; Holmes, A. B.; Burroughes, J. H.; Marks, R. N.; Taliani, C.; Bradley, D. D. C.; Santos, D. A. D.; Bredas, J. L.; Logdlund, M.; Salaneck, W. R. *Nature* **1999**, *397*, 121.

(9) Dimitrakopoulos, C. D.; Malenfant, P. R. L. *Adv. Mater.* **2002**, *14*, 99.

(10) John K, B. *Mater. Today* **2004**, *7*, 42.

(11) Chiang, C. K.; Fincher, C. R., Jr.; Park, Y. W.; Heeger, A. J.; Shirakawa, H.; Louis, E. J.; Gau, S. C.; MacDiarmid, A. G. *Phys. Rev. Lett.* **1977**, *39*, 1098.

(12) Pope, M.; Kallmann, H. P.; Magnante, P. *J. Chem. Phys.* **1963**, *38*, 2042.

(13) Tang, C. W.; VanSlyke, S. A. *Appl. Phys. Lett.* **1987**, *51*, 913.

(14) Burroughes, J. H.; Bradley, D. D. C.; Brown, A. R.; Marks, R. N.; Mackay, K.; Friend, R. H.; Burns, P. L.; Holmes, A. B. *Nature* **1990**, *347*, 539.

(15) Freundenrich, C. In *HowStuffWorks* 2005.

(16) Brédas, J.-L.; Beljonne, D.; Coropceanu, V.; Cornil, J. *Chem. Rev.* **2004**, *104*, 4971.

(17) Shaheen, S. E.; Ginley, D. S.; Jabbour, G. E. *MRS Bulletin* **2005**, *30*, 10.

(18) Chapin, D. M.; Fuller, C. S.; Pearson, G. L. *J. Appl. Phys.* **1954**, *25*, 676.

(19) Forrest, S. R. *MRS Bulletin* **2005**, *30*, 28.

(20) Sariciftci, N. S.; Smilowitz, L.; Heeger, A. J.; Wudl, F. *Science* **1992**, *258*, 1474.

(21) Crone, B. K. *J. Appl. Phys.* **2001**, *91*, 10140.

(22) Bartic, C.; Campitelli, A.; Borghs, G. *Appl. Phys. Lett.* **2003**, *82*, 475.

(23) Rogers, J. A. *Proc. Natl. Acad. Sci. USA* **2001**, *98*, 4835.

(24) Sheraw, C. D. *Appl. Phys. Lett.* **2002**, *80*, 1088.

(25) Huitema, H. E. A. *Nature* **2001**, *414*, 599.

(26) Gelinck, G.; Heremans, P.; Nomoto, K.; Anthopoulos, T. D. *Adv. Mater.* **2010**, *22*, 3778.

(27) Novak, M.; Jäger, C. M.; Rumpel, A.; Kropp, H.; Peukert, W.; Clark, T.; Halik, M. *Org. Electron.* **2010**, *11*, 1476.

(28) Halik, M.; Klauk, H.; Zschieschang, U.; Schmid, G.; Dehm, C.; Schutz, M.; Maisch, S.; Effenberger, F.; Brunnbauer, M.; Stellacci, F. *Nature* **2004**, *431*, 963.

(29) Arita, T.; Moriya, K.; Yoshimura, T.; Minami, K.; Naka, T.; Adschiri, T. *Ind. Eng. Chem. Res.* **2010**, *49*, 9815.
(30) Ganbold, E. O.; Lee, Y.; Lee, K.; Kwon, O.; Joo, S. W. *Chem. Asian. J.* **2010**, *5*, 852.
(31) Arita, T.; Moriya, K.; Minami, K.; Naka, T.; Adschiri, T. *Chem. Lett.* **2010**, *39*, 961.
(32) Luschtinetz, R.; Frenzel, J.; Milek, T.; Seifert, G. *J. Phys. Chem. C* **2009**, *113*, 5730.
(33) Jedaa, A.; Burkhardt, M.; Zschieschang, U.; Klauk, H.; Habich, D.; Schmid, G.; Halik, M. *Org. Electron.* **2009**, *10*, 1442.
(34) Habich, D. B.; Halik, M.; Schmid, G. *Thin Solid Films* **2011**, *519*, 7809.
(35) Hagberg, D. P.; Marinado, T.; Karlsson, K. M.; Nonomura, K.; Qin, P.; Boschloo, G.; Brinck, T.; Hagfeldt, A.; Sun, L. *J. Org. Chem.* **2007**, *72*, 9550.
(36) Xu, W.; Peng, B.; Chen, J.; Liang, M.; Cai, F. *J. Phys. Chem. C* **2008**, *112*, 874.
(37) Schulmeyer, T.; Paniagua, S. A.; Veneman, P. A.; Jones, S. C.; Hotchkiss, P. J.; Mudalige, A.; Pemberton, J. E.; Marder, S. R.; Armstrong, N. R. *J. Mater. Chem.* **2007**, *17*, 4563.
(38) Kim, P.; Jones, S. C.; Hotchkiss, P. J.; Haddock, J. N.; Kippelen, B.; Marder, S. R.; Perry, J. W. *Adv. Mater.* **2007**, *19*, 1001.
(39) Breen, T. L.; Fryer, P. M.; Nunes, R. W.; Rothwell, M. E. *Langmuir* **2001**, *18*, 194.
(40) Kresse, G.; Furthmüller, J. *Comput. Mat. Sci.* **1996**, *6*, 15.
(41) Kresse, G.; Furthmüller, J. *Phys. Rev. B* **1996**, *54*, 11169.
(42) Perdew, J. P.; Burke, K.; Ernzerhof, M. *Phys. Rev. Lett.* **1996**, *77*, 3865.
(43) Perdew, J. P.; Burke, K.; Ernzerhof, M. *Phys. Rev. Lett.* **1997**, *78*, 1396.
(44) Blöchl, P. E. *Phys. Rev. B* **1994**, *50*, 17953.
(45) Dudarev, S. L.; Botton, G. A.; Savrasov, S. Y.; Humphreys, C. J.; Sutton, A. P. *Phys. Rev. B* **1998**, *57*, 1505.
(46) Palacios, P.; Sanchez, K.; Wahnon, P. *Thin Solid Films* **2009**, *517*, 2448.
(47) Li, H.; Schirra, L. K.; Group), K.; Kippelen, B.; Monti, O. L. A.; Bredas, J.-L. **2012**.
(48) Srikant, V.; Clarke, D. R. *J. Appl. Phys.* **1998**, *83*, 5447.
(49) Pehlke, E.; Scheffler, M. *Phys. Rev. Lett.* **1993**, *71*, 2338.
(50) Köhler, L.; Kresse, G. *Phys. Rev. B* **2004**, *70*, 165405.
(51) Uhlrich, J. J.; Olson, D. C.; Hsu, J. W. P.; Kuech, T. F. *J. Vac. Sci. Technol. A* **2009**, *27*, 328.
(52) Moormann, H.; Kohl, D.; Heiland, G. *Surf. Science* **1980**, *100*, 302.
(53) Chen, L.-M.; Xu, Z.; Hong, Z.; Yang, Y. *J. Mater. Chem.* **2010**, *20*, 2575.
(54) Olson, D. C.; Shaheen, S. E.; Collins, R. T.; Ginley, D. S. *J. Phys. Chem. C* **2007**, *111*, 16670.
(55) Chen, S.; Deng, L.; Xie, J.; Peng, L.; Xie, L.; Fan, Q.; Huang, W. *Adv. Mater.* **2010**.
(56) Wei, A.; Pan, L. H.; Huang, W. *Mater. Sci. Eng. B* **2011**, *176*, 1409.

(57) Salaneck, W.; Seki, K.; Kahn, A.; Pireaux, J. J. *Conjugated Polymers and Molecular Interfaces: Science and Technology for Photonic and Optoelectronic Applications*, 2002.

(58) Ishii, H.; Sugiyama, K.; Ito, E.; Seki, K. *Adv. Mater.* **1999**, *11*, 605.

(59) Chen, W.; Huang, C.; Gao, X. Y.; Wang, L.; Zhen, C. G.; Qi, D. C.; Chen, S.; Zhang, H. L.; Loh, K. P.; Chen, Z. K.; Wee, A. T. S. *J. Phys. Chem. B* **2006**, *110*, 26075.

(60) Allen, C. G.; Baker, D. J.; Albin, J. M.; Oertli, H. E.; Gillaspie, D. T.; Olson, D. C.; Furtak, T. E.; Collins, R. T. *Langmuir* **2008**, *24*, 13393.

(61) Ozawa, K.; Hasegawa, T.; Edamoto, K.; Takahashi, K.; Kamada, M. *J. Phys. Chem. B* **2002**, *106*, 9380.

(62) Lopes Martins, J. B.; Longo, E.; RodrIguez Salmon, O. D.; Espinoza, V. A. A.; Taft, C. A. *Chem. Phys. Lett.* **2004**, *400*, 481.

(63) Thomsen, L.; Watts, B.; Dastoor, P. C. *Surf. Interface Anal.* **2006**, *38*, 1139.

(64) Nogues, C.; Lang, P. *Langmuir* **2007**, *23*, 8385.

(65) Rhodes, C. L.; Lappi, S.; Fischer, D.; Sambasivan, S.; Genzer, J.; Franzen, S. *Langmuir* **2008**, *24*, 433.

(66) Sadik, P. W.; Pearton, S. J.; Norton, D. P.; Lambers, E.; Ren, F. *J. Appl. Phys.* **2007**, *101*, 104514.

(67) Persson, P.; Lunell, S.; Ojamäe, L. *Int. J. Quantum Chem.* **2002**, *89*, 172.

(68) Chen, Y. S.; Li, C.; Zeng, Z. H.; Wang, W. B.; Wang, X. S.; Zhang, B. W. *J. Mater. Chem.* **2005**, *15*, 1654.

(69) Labat, F.; Ciofini, I.; Hratchian, H. P.; Frisch, M.; Raghavachari, K.; Adamo, C. *J. Am. Chem. Soc.* **2009**, *131*, 14290.

(70) Moreira, N. H.; da, R. A. L.; Frauenheim, T. *Appl. Phys. Lett.* **2009**, *94*, 193109/1.

(71) Tian, X.; Xu, J.; Xie, W. *J. Phys. Chem. C* **2010**, *114*, 3973.

(72) Domínguez, A.; Moreira, N. H.; Dolgonos, G.; Frauenheim, T.; da Rosa, A. L. *J. Phys. Chem. C* **2011**, null.

(73) Yip, H. L.; Hau, S. K.; Baek, N. S.; Jen, A. K. Y. *Appl. Phys. Lett.* **2008**, *92*, 193313.

(74) Paukku, Y.; Michalkova, A.; Leszczynski, J. *J. Phys. Chem. C* **2009**, *113*, 1474.

(75) Zhang, B.; Kong, T.; Xu, W.; Su, R.; Gao, Y.; Cheng, G. *Langmuir* **2010**, *26*, 4514.

(76) Hotchkiss, P. J.; Malicki, M.; Giordano, A. J.; Armstrong, N. R.; Marder, S. R. *J. Mater. Chem.* **2011**, *21*, 3107.

(77) Guerrero, G.; Mutin, P. H.; Vioux, A. *Chem. Mater.* **2001**, *13*, 4367.

(78) Nie, H. Y.; Walzak, M. J.; McIntyre, N. S. *J. Phys. Chem. B* **2006**, *110*, 21101.

(79) Cui, J.; Huang, Q.; Veinot, J. G. C.; Yan, H.; Marks, T. J. *Adv. Mater.* **2002**, *14*, 565.

(80) Yan, H.; Lee, P.; Graham, A.; Armstrong, N. R.; Evmenenko, G. A.; Dutta, P.; Marks, T. J. *J. Am. Chem. Soc.* **2005**, *127*, 3172.

(81) Ma, H.; Yip, H. L.; Huang, F.; Jen, A. K. Y. *Adv. Funct. Mater.* **2010**, *20*, 1371.

(82) Armstrong, N. R.; Veneman, P. A.; Ratcliff, E.; Placencia, D.; Brumbach, M. *Acc. Chem. Res.* **2009**, *42*, 1748.

(83) Paramonov, P. B.; Paniagua, S. A.; Hotchkiss, P. J.; Jones, S. C.; Armstrong, N. R.; Marder, S. R.; Brédas, J.-L. *Chem. Mater.* **2008**, *20*, 5131.

(84) Hotchkiss, P. J.; Jones, S. C.; Paniagua, S. A.; Sharma, A.; Kippelen, B.; Armstrong, N. R.; Marder, S. R. *Acc. Chem. Res.* **2011**.

(85) Chen, Y. F.; Kim, M.; Lian, G.; Johnson, M. B.; Peng, X. G. *J. Am. Chem. Soc.* **2005**, *127*, 13331.

(86) Wei, T.; Jin, C. Q.; Zhong, W.; Liu, J.-M. *Appl. Phys. Lett.* **2007**, *91*, 222907.

(87) Sinapi, F.; Forget, L.; Delhalle, J.; Mekhalif, Z. *Surf. Interface Anal.* **2002**, *34*, 148.

(88) Perkins, C. L. *J. Phys. Chem. C* **2009**, *113*, 18276.

(89) Gouzman, I.; Dubey, M.; Carolus, M. D.; Schwartz, J.; Bernasek, S. L. *Surf. Sci.* **2006**, *600*, 773.

(90) Gawalt, E. S.; Avaltroni, M. J.; Koch, N.; Schwartz, J. *Langmuir* **2001**, *17*, 5736.

(91) Pellerite, M. J.; Dunbar, T. D.; Boardman, L. D.; Wood, E. J. *J. Phys. Chem. B* **2003**, *107*, 11726.

(92) Giza, M.; Thissen, P.; Grundmeier, G. *Langmuir* **2008**, *24*, 8688.

(93) Schulmeyer, T.; Paniagua, S. A.; Veneman, P. A.; Jones, S. C.; Hotchkiss, P. J.; Mudalige, A.; Pemberton, J. E.; Marder, S. R.; Armstrong, N. R. *J. Mater. Chem.* **2007**, *17*, 4563.

(94) Gao, W.; Dickinson, L.; Grozinger, C.; Morin, F. G.; Reven, L. *Langmuir* **1996**, *12*, 6429.

(95) Kohl, D.; Moorman, H.; Heiland, G. *Surf. Science* **1978**, *73*, 160.

(96) Alloway, D. M.; Hofmann, M.; Smith, D. L.; Gruhn, N. E.; Graham, A. L.; Colorado, R.; Wysocki, V. H.; Lee, T. R.; Lee, P. A.; Armstrong, N. R. *J. Phys. Chem. B* **2003**, *107*, 11690.

(97) Hotchkiss, P. J.; Li, H.; Paramonov, P. B.; Paniagua, S. A.; Jones, S. C.; Armstrong, N. R.; Brédas, J.-L.; Marder, S. R. *Adv. Mater.* **2009**, *21*, 4496.

(98) Li, H.; Paramonov, P.; Brédas, J.-L. *J. Mater. Chem.* **2010**, *20*, 2630.

(99) Heimel, G.; Romaner, L.; Zojer, E.; Bredas, J. L. *Nano Lett.* **2007**, *7*, 932.

(100) Heimel, G.; Rissner, F.; Zojer, E. *Adv. Mater.* **2010**, *22*, 2494.